Universidade de Lisboa
Faculdade de Ciências
Departamento de Biologia Vegetal

Super-Resolution Imaging of the Structural Maintenance of Chromosome (SMC) complexes Cohesin and Condensin

Pedro Manuel Bento Carvalho Almada

Dissertação de Mestrado
Mestrado em Biologia Celular e Biotecnologia

2013

Universidade de Lisboa
Faculdade de Ciências
Departamento de Biologia Vegetal

Super-Resolution Imaging of the Structural Maintenance of Chromosome (SMC) complexes Cohesin and Condensin

Pedro Manuel Bento Carvalho Almada

Dissertação de Mestrado orientada pelo Prof. Doutor Gabriel Martins da Faculdade de Ciências e pela Doutora Raquel Oliveira do Instituto Gulbenkian de Ciência

Mestrado em Biologia Celular e Biotecnologia

2013

Resumo

Os complexos proteicos "*Structural Maintenance of Chromosomes"* (SMC) têm papéis importantes na estrutura cromossómica. Destes, destacam-se a coesina e as condensinas. A coesina mantém os cromatídeos irmãos unidos de modo a permitir a sua fiel segregação enquanto que as condensinas são principalmente responsáveis pela condensação dos cromossomas em preparação para a divisão celular[1]. A distribuição destes complexos no cromossoma e a sua interacção com outras proteínas associadas ao ADN é actualmente alvo de intensa investigação. Quando os cromossomas estão condensados sabe-se que a condensina aparece num eixo restrito ao longo dos cromatídeos. Sabe-se também que neste período as coesinas estão localizadas maioritariamente na região pericentromérica. Mas não é ainda conhecido se a sua distribuição abrange toda a largura da do centrómero ou, para os dois complexos, se têm uma distribuição restrita centralmente, se pontual ou difusa (figura 3). O limite para perceber a sua distribuição é resultado do limite de resolução das técnicas tradicionais de microscopia óptica. Estas estão limitadas pela difracção da luz a uma resolução de cerca de 200 nm. Embora a microscopia electrónica consiga maior resolução, esta não permite discriminar os complexos de forma selectiva do restante contexto celular[2]. Como tal, o desenvolvimento de ferramentas que consigam determinar a sua distribuição com maior fiabilidade permitirá novas avenidas de investigação.

Com este trabalho monstramos o desenvolvimento de um sistema de microscopia de super-resolução e conjunto de protocolos capazes de obter imagens de super-resolução dos complexos SMC em células de *Drosophila melanogaster*.

Das técnicas que permitem maior resolução desenvolvidas actualmente, as que se baseiam na localização de moléculas individuais (SML, sigla inglesa) são as mais simples de implementar a nível de *hardware*[2]. Estas são baseadas no princípio de que a posição de uma molécula pode ser identificada com maior precisão do que a resolução do microscópio. Isto é apenas possível se a molécula estiver individualizada, permitindo que se faça um ajuste a uma curva gaussiana bidimensional a cada fluoróforo individual. Numa amostra fluorescente normal, todos os fluoróforos emitem simultaneamente o que impede a sua discriminação. As diferenças nas variadas técnicas de SML residem na forma de conseguir que apenas uma fracção reduzida dos fluoróforos emita em determinado período de tempo. A técnica de dSTORM baseia-se no facto de que a maioria dos fluoróforos, após excitação com um laser suficientemente forte, entra

num estado em que não emitem luz com duração de alguns milissegundos a várias dezenas de segundos. Se for obtido um filme da amostra enquanto esta é exposta à luz de um laser suficientemente intensa, iremos obter um filme dos fluoróforos a piscar. Poderemos então analisar com um algoritmo de localização o filme e identificar todos os fluoróforos presentes na amostra. No final, uma imagem de super-resolução pode ser obtida pela reconstrução dos pontos que foram localizados, pois a sua localização é feita com maior precisão do que a resolução teórica do microscópio[3]. Um sistema dSTORM, no geral, apenas precisa de um microscópio convencional e um laser suficientemente forte, o que simplifica a sua implementação. Dada a simplicidade dos requerimentos, optou-se por montar um sistema dSTORM para obter imagens dos complexos SMC. Foi obtido um microscópio Nikon com uma objectiva de 100x e 1.45 de abertura numérica (permitindo a melhor colecção de sinal da amostra possível), dado que a precisão da localização depende da quantidade de fotões capturados. A este microscópio foi adaptado um laser de 639nm de comprimento de onda KVANT com 166 mW de potência, permitindo a indução dos estados não-emissores nos fluoróforos presentes na amostra. Simultaneamente foram estabelecidas formas de preparação de amostra que permitam a melhor imagem possível para dSTORM.

Principalmente, visto que a espessura da amostra também afecta a qualidade da colecção, foi estabelecido um protocolo para obter preparações de cromossomas em lamelas utilizando o sistema Cytospin. Este consiste numa centrífuga com suportes para lâminas e funis que aceitam as células; quando começa a centrifugar, as células são projectadas na lâmina de modo a obter amostras tão planas quanto possível. Quando as células são tratadas com uma solução hipotónica, o núcleo é rompido e os cromossomas separados.

Outra alteração importante ao protocolo normal de imunofluorescência foi a adição de um segundo passo de fixação, no final do protocolo. Isto porque com a exposição a uma fonte de luz de elevada potência (p.ex. um laser) alguns dos fluoróforos destacam-se dos anticorpos a que estão ligados (Ricardo Henriques, comunicação pessoal).

Finalmente, em todos os microscópios existe a chamada deriva térmica. Qualquer amostra observada ao microscópio, irá estar a uma temperatura ligeiramente diferente e a sua diferença será equilibrada pela platina que a segura. Dado que a platina e a objectiva costumam ser peças independentes e de materiais diferentes, a amostra irá ser deslocada muito ligeiramente pela deriva térmica da platina ao longo do tempo. Esta deriva é de um valor muito pequeno, mas

no decurso de uma aquisição de uma sequência de imagens para subsequente localização, afecta significativamente a reconstrução, a menos que seja corrigida. Para resolver este problema podem incluir-se marcadores na amostra que são depois usados como referência para o algoritmo de reconstrução; este mede a deriva dos marcadores e corrige na tabela de localizações dos pontos. No nosso caso, incluímos sempre microesferas fluorescentes Tetraspeck de 100 nanómetros de diâmetro, que é abaixo da resolução do microscópio. Esta correcção apenas corrige deriva no plano lateral do microscópio, mas o microscópio obtido possui um sistema de correcção de *hardware* da deriva axial que consegue manter a amostra em foco durante a aquisição.

Com este sistema e a nova preparação de amostra, obtivemos imagens de super-resolução da proteína Rad21, uma subunidade da coesina (Figura 10). As reconstruções de Rad21 obtidas mostraram que a proteína se localiza numa zona axialmente restrita com uma largura de sensivelmente 85 nm, consideravelmente abaixo da resolução do microscópio. Vários modelos têm sido descritos para o modo como as coesinas promovem a coesão entre os cromatídios (Figura 2). Destes, o nosso resultado favorece o modelo em que um único anel aprisiona os dois cromatídeos irmãos. Por oposição, este resultado vai contra um modelo alternativo que propõe que dois anéis de coesina estão envolvidos na coesão, cada um rodeando um dos cromatídeos irmãos (Figura 2d). Com este modelo, seria de esperar distribuições de 100 ou mais nanómetros dado que cada anél tem 50 nm de comprimento e estas localizações têm ainda a contribuição do comprimento dos dois anticorpos usados para fazer a marcação (10 a 15 nm cada).

Estes resultados, embora promissores, carecem de futura optimização e confirmação uma vez que encontrámos estruturas não-específicas fora dos cromossomas e dos núcleos. Provavelmente estas estruturas devem-se a aglomeração do anticorpo secundário ou a ligação não-específica a proteínas presentes na preparação. De futuro será benéfico efectuar as marcações com fragmentos de anticorpos marcados com fluoróforos orgânicos. Estes são mais específicos e produzem marcações com menos ruído-de-fundo que os anticorpos policlonais tradicionais[4]. Também são moleculas menores, o que permite diminuir o erro de localização associado à introdução de vários anticorpos de ~10 nanómetros de tamanho na amostra[5]. Efectivamente, existem fragmentos de anticorpos contra GFP e, o laboratório consegue obter células com marcação GFP em cultura. Também será viável a criação de culturas primárias de cérebros de larvas de drosophila que têm uma percentagem elevada de células em divisão. Estas

culturas primárias permitiria aproveitar a diversidade de linhas com marcação GFP existentes no laboratório.

Também era objectivo deste trabalho abordar as Condensinas, mas não foi possível dentro do tempo disponível devido a limitações técnicas.

Em resumo, descrevemos aqui um sistema e conjunto de protocolos que consegue obter imagens de super-resolução de pelo menos um dos complexos SMC. Imediatamente foi feita uma observação que permite começar a descartar um dos modelos prevalentes propostos para a organização das coesinas e acreditamos que estes são os primeiros passos para um sistema que consiga no futuro obter mais respostas sobre a função e organização dos complexos SMC.

Abstract

The protein complexes of the "*Structural Maintenance of Chromosomes"* family have important roles on chromosome structure: cohesin binds sister-chromatids together in order to allow their faithful segregation, and the condensins are responsible for chromosome condensation ahead of cell division, amongst other functions. Their structural distribution along DNA and their interaction with other DNA-bound proteins is currently the subject of intense investigations. This means that the development of tools which are able to determine the distribution of these complexes with greater reliability will allow new avenues of research.

We have developed a super-resolution microscopy system and protocols capable of obtaining super-resolution images of the SMC complexes in Drosophila melanogaster cells. With this system we have successfully obtained images of the Rad21 subunit of cohesin and could demonstrate that it is restricted to a small axially defined region demarcating both sister-chromatids. In short, we present a system and protocols which can start to provide answers on the localization and function of the SMC complexes.

Portuguese Keywords

Super-Resolução; dSTORM; Structural Maintenance of Chromosomes; Coesina; Condensina; *cytospin*; *Drosophila melanogaster*

English Keywords

Super-Resolution; dSTORM; Structural Maintenance of Chromosomes; Cohesin; Condensin; cytospin; *Drosophila melanogaster*

Acknowledgments

I would like to thank my supervisors, Raquel Oliveira and Gabriel Martins, for all their help and assistance. I would also like to acknowledge and thank for the help and assistance given by Ricardo Henriques with the dSTORM design and methods; Emilio Gualda with the optical set-up; Mihailo Mirkovic and Ewa Piskadlo for generous help with sample preparations and Nuno Moreno for his support and guidance during the project.

Table of Contents

Introduction

Chromosomal DNA is a massive molecule which, if stretched end-to-end, can reach two meters in length[6]. Packing such a long, linear molecule in the confined space of the nucleus is a non-trivial matter. This challenge is further increased at the time of nuclear division, as chromosomes need to be further compacted to make chromosome segregation feasible within the cell space. The cell also needs to be able to correctly identify the sister of each chromatid in order to provide the correct complement of chromosomes to each daughter cells.

The Structural Maintenance of Chromosome (SMC) Complexes

Faithful segregation of chromatids during cell division is thought to be the result of the combination of compaction of the chromosomes and sister-chromatid cohesion[7]. The Structural Maintenance of Chromosomes (SMC) family of protein complexes contains key players for both processes. These complexes are composed of two SMC proteins, a Kleisin subunit and other functional subunits. The two SMC proteins have a coiled coil conformation and are roughly 50 nanometers long. They heterodimerize through the central "hinge" domain of each SMC protein. The N- and C- termini are joined together in what is called the "head" domain and bind to different regions of a Kleisin protein while the remaining subunits interact with this Kleisin protein. The overall shape of the complex is that of a ring (Figure 1). The head domains are joined together by an ATP binding site which is sandwiched between both when the domain is in a closed conformation[8].

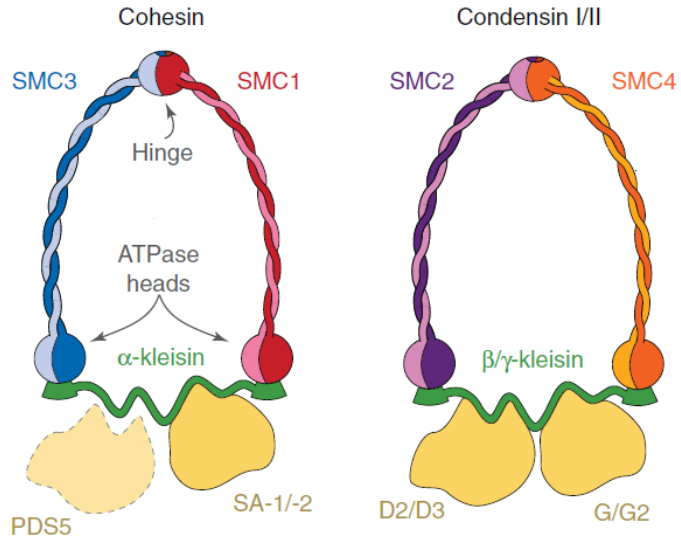

Figure 1 - The SMC complexes. Diagram adapted from Cuylen & Haering, 2011[8].

Three major complexes have been identified: Cohesin and Condensin I and II. These complexes have a ring-like structure composed of two proteins of the SMC family linked end-to-end and a Kleisin protein linking the opposing ends (Figure 1)[8]. A related complex has also been identified (SMC5/6 complex) but it is primarily involved in DNA repair and therefore does not contribute to chromosome

morphology specifically during mitosis[1].

Cohesins and sister chromatid cohesion

In order to discriminate each chromatid pair, sister-chromatids are bound together as soon as the DNA of the cell is replicated during S phase. This pairing is maintained until mitosis or meiosis and is essential to prevent random chromosome segregation during nuclear division. During prometaphase, when the microtubules attach to the chromosomes, the sister-chromatids align along the metaphase plate and it is this that permits the correct segregation of chromatids during metaphase. By the time cells reach metaphase, the chromosome arms are mostly resolved and only a small area surrounding the centromeres is promoting sister chromatid cohesion.

Cohesin has been shown to be required for chromatid cohesion. It is a complex composed of SMC1, SMC3, Scc1 (α-Kleisin), and Scc3 and given its ring-like shape one would expect its function to be the result of a topological interaction with DNA. There is evidence that this is true. For example, proteolytically cleaving Scc1 in flies abolishes sister-chromatid resolution completely within minutes[9]. Moreover, chemical crosslinking of cohesin embracing circular chromosomes leads to cohesin-DNA complexes that are resistant to SDS denaturation[10] which further supports a topological embracement model. Cohesin's interaction with DNA is relatively well established but questions still remain on its overall structure in the chromatin. For example, does cohesin hold both sister-chromatids within a single ring or does cohesion result from

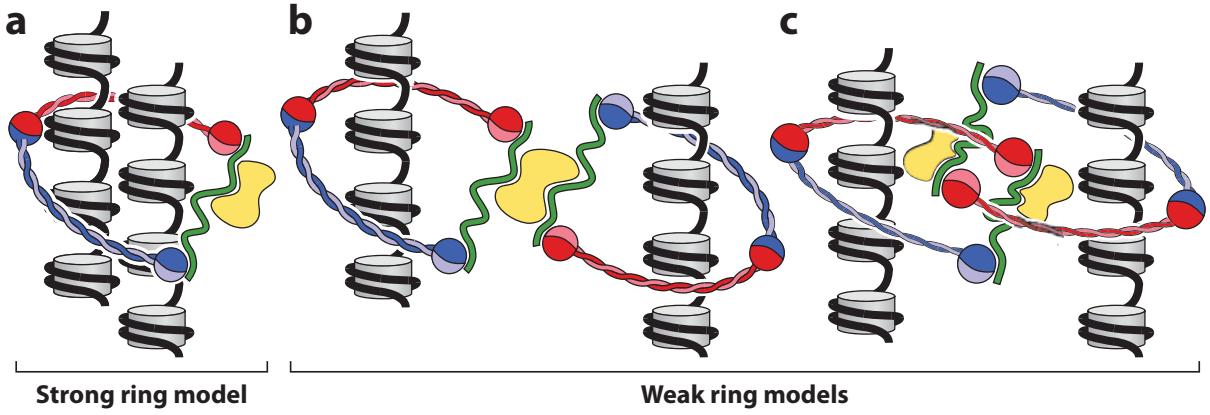

Figure 2 - Sister chromatid cohesion models by cohesin rings. Diagram adapted from Nasmyth & Haering 2009[6] A - The strong version of the ring model sees the DNA as being trapped inside a single cohesin ring. B - The handcuff model proposes that the two tripartite Smc1/3/Scc1 rings are held together by Scc3. C - Another possible weak model states that the rings embrace a single strand of DNA as well as its sisters' ring.

entrapment of two cohesin rings, each embracing a single chromatid[6] (*Figure* 2)? Additionally, although we know cohesin to be enriched at the pericentromeric region[6] it is not yet clear where within the mitotic chromosome do they locate. Are they present all over the centromeric region (Figure 3a) or are cohesive regions restricted to the most inner part of mitotic chromosomes (Figure 3c)? Are there stretches of cohesin linking particular areas (Figure 3b), or is it more distributed more diffusely (Figure 3a)? Answering these questions will be important to further elucidate how these complexes promote sister chromatids together and also how the overall chromosome organization is achieved.

Condensins and mitotic chromosome organization

Mitotic chromosome organization ensures several changes in chromatin organization to fulfill many purposes: 1) Chromosomes need to be more compacted than in interphase to allow their efficient segregation; 2) Chromosome arms need to be resolved so that sister chromatids are properly disjoined; 3) Chromosomes need to acquire the right mechanical properties to favor their movements during mitosis (alignment at the metaphase plate and subsequent segregation to

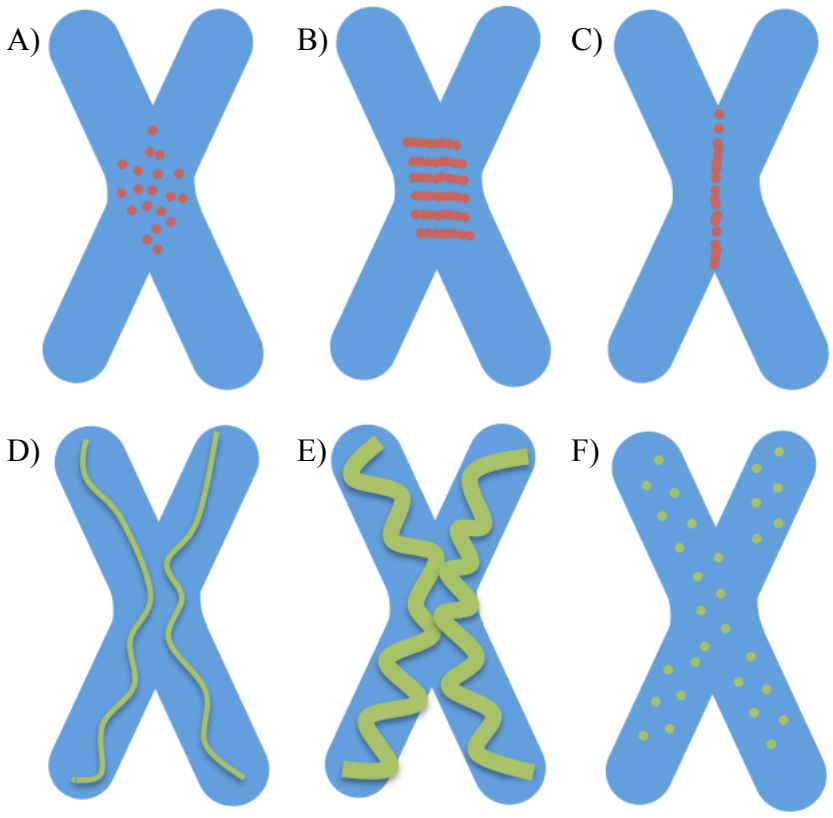

Figure 3 – Different models for the localization of the SMC complexes (A to C, cohesin models; D to E, condensin models).

the poles). Condensin complexes have been proposed to be at the heart of most of these chromosomal changes. Condensin I and II are both composed of SMC2 and 4 and either a γ- (Condensin I) or β- Kleisin (Condensin II). Additionally they contain two non-SMC proteins (CAP-G2/3 and CAP-D1/2). Condensin I has been demonstrated to be the protein involved in chromosome condensation in preparation for cell division[8]. Condensin II's role is yet to be properly defined but seems to also have a role in the compaction of chromosomes, as well as other functions[8].

Condensins are known to localize to a central axis within each sister chromatid and are thought to be capable of organizing chromatin loops in order to promote the resolution of sister chromatids[8]. Condensins are also the most abundant complexes of the chromosome scaffold, a protein structure that retains the chromosome size and shape even after histone removal[11]. They have therefore been proposed to hold chromatin loops at the center of sister chromatids. The nature of the topological interaction with DNA of the Condensin complexes is still the subject of speculation in current research, with different models having different followers. Condensin I has been shown to be a dynamic molecule through FRAP experiments in fly embryos[12] and human cells[13] which raises questions on its viability as a structural scaffold for the DNA as has been thought[8]. It is still possible that condensins act as (dynamic) scaffolds but their mode of function is clearly more complex. In particular, it would be important to understand how does the morphology of the inner axis organized by condensins relate to the overall chromosome shape. Do condensins form a continuous axis in which cooperative interactions promote chromosome shortening (Figure 3e,f)? Are condensin complexes accumulated at the center of chromatid in a non-continuous manner (Figure 3f)? Further dissection on condensins localization within the mitotic chromosome along with a better understating of the structure of the chromosome axis organized by condensins will be pivotal for the understanding of condensins' mode of action and the process of chromosome condensation.

Super-resolution imaging of mitotic chromosomes

$$Eq.1)\ R = \frac{\lambda}{NAO + NAC} \qquad Eq.2)\ R = \frac{1.22\,\lambda}{NAO + NAC}$$

Equations 1 & 2 - Rayleigh and Abbe's equations for their criteria of resolution. R stands for minimum resolvable distance between two points, or resolution; NAO stands for numerical aperture of the objective; NAC stands for numerical aperture of the condenser; λ is the wavelength of the collected electromagnetic radiation.

It is then useful to develop new techniques and methods, which are able to resolve these structures with finer detail and molecular specificity. Traditional microscopy is limited in how well it can resolve structures by two properties: the wavelength of the light being imaged and the numerical aperture of the collection objective. This is because any electromagnetic radiation is diffracted when it travels through the lenses of the microscope, which act as apertures[14,15]. Two infinitely small points of light which are collected with an objective and focused on the image plane of the microscope will have to be at least 200nm apart to be properly discriminated, depending on which criterion used to define resolution. A few empirically determined equations have been developed in different contexts. In the late 19th century, Ernst Abbe, a physicist working for Zeiss who was trying to determine the resolution of their transmitted light microscopes derived equation 1[16]. For an objective and condenser with a numerical aperture of 1.4, trying to image a sample using green light (with a wavelength of 560nm), this equation yields the previously mentioned value of 200nm. Also in the 19th century, Lord Rayleigh measured the resolution of his telescope when trying to image far away stars in the dark night sky, which can be approximated to infinitely small points of light. In his studies he empirically derived equation 2 which yields a slightly lower resolution of 244nm in the same case described above[17]. However, both equations are strikingly similar and clearly show that the only two important parameters for resolution are the wavelength of the collected electromagnetic radiation (i.e. light, x-rays, electrons) and the numerical aperture of the imaging system. The choice of which criterion to use is subjective and both are commonly used in the literature to measure resolution. Rayleigh's criterion is often used with the argument that bright spots on a dark background are closer to the case of fluorescence microscopy. Still, most microscopy images will not be near the theoretical limit unless the sample preparation and microscope parts are close to perfect.

Either equation can also be used to calculate the resolution of electron microscopy, given that the diffraction affects electrons as well. The wavelength of an electron depends on its momentum, but for a 10kV microscope, an electron is expected to have 12.2 pm, several orders of magnitude smaller than the wavelength of a photon. This explains the enhanced resolution of the electron microscope. Unfortunately, it's extremely difficult to correct the aberrations present in an electron microscope's lenses. This means that, on a regular basis, a transmission electron microscope should reach around 10nm resolution[18]. The TEAM project in the united states has produced a microscope which is highly corrected and they have reported the ability to resolve down to 0.5 nm, meaning they have been able to resolve single carbon molecules in graphene sheets[19]. But at this range, the samples have to be able to endure extreme amounts of energy, which renders the technique mostly incompatible with biological samples. One other issue with electron microscopy is that the contrast is due to electron absorption, a feature very few molecules possess in reasonable amount to be discernible. Further specificity can be achieved with immuno-gold labeling, but it is technically difficult. Specificity is the main feature of fluorescence microscopy. Either by tagging a protein genetically, with a fluorescently labeled antibody or other form of dye, the pictures will, usually, only show the structure of interest. This is important in the context of the cell given the vast amount of different molecules present. As it is an optical technique, it is limited by the resolution afforded by the wavelength of photons. In order to and provide increases of resolution up to 20 nm. Appropriately, these techniques have been dubbed Super-Resolution techniques[2].

Three major Super-Resolution techniques have become widespread: Structured Illumination Microscopy (SIM), Saturated Emission Depletion (STED) microscopy and Single Molecule Localization (SML). All of these can reach resolutions in the tens of nanometers. SML is based on identifying single fluorophores using a standard widefield microscope (Sup. Fig. 1) in contrast to SIM and STED, which require complex optical systems[20]. SML microscopy is based on the insight that, if a single fluorophore can be imaged, its localization can be estimated by fitting a 2D Gaussian function and calculating its center. This localization can be made with a precision greater than the resolution of the microscope, dependent only on the amount of photons, which can be collected. With sufficient photons collected, resolutions of 20 nm can be achieved on a regular basis[2]. The different variations of the technique reside on how to make only single molecules visible since, on a common fluorescent sample, all fluorophores will be

emitting at the same time. PALM (Photo-Activated Localization Microscopy) is based on genetically tagged proteins, which can be photo-activated or photo-switched, like Dronpa or mEOS2. By exposing them to light of a certain wavelength, these proteins can switch between a non-emitting state and emitting in a wavelength different from the one that will be collected. By flashing light of another wavelength, a sparse random selection of the molecules will emit again in the desired wavelength. These are imaged and then bleached with UV light, so that a new selection can be activated, imaged and bleached. This is repeated over several thousand cycles in order to be able to pinpoint enough molecules to reconstruct the structure of interest with sufficient fidelity[2].

In dSTORM (direct Stochastic Optical Reconstruction Microscopy) fluorophores are made to blink naturally. While most fluorophores emit light continuously until bleached, they can also enter so called dark-states, where they are not bleached, but are also not emitting any light. These states are reversible but long-lasting. Shining a large amount of photons on the fluorophore can induce them into these dark-states. Because these dark-states can be in the order of hundreds of milliseconds[3], resulting in very few fluorophores emitting for each exposure, the addition of certain thiols such as β-mercaptoethanol or beta-mercaptoethylamine promotes recovery from the dark-states into emitting states. The amount of fluorophores that are in an emitting state at a given time can be modulated by varying the concentration of these thiols. STORM also usually uses organic dyes, either rhodamines (Alexa647 is a commercial example) or cyanines (for example Cy5). This is because these species will enter dark-states with lower laser powers than most other fluorophores but also because they have a higher quantum yield and absorption cross-section than most protein fluorophores like EGFP, resulting in more emitted photons and, therefore, greater resolution with the localization algorithms[2,21].

Of the three major techniques, SML microscopy has relatively simple hardware requirements[22]. Because of the power and speed required for PALM, three lasers are necessary (for activation, imaging and bleaching) but there is no need for special alignment procedures or complex beam shaping[20,22]. DSTORM is even simpler, requiring only one powerful laser for each wavelength to be analyzed. Everything else that is required for either technique is a fairly standard microscope and a sensitive camera. Most modern cell biology labs will have access to microscopes with such cameras, which means that what is usually missing is a powerful laser. The remaining requirements lie in the choice of fluorophores to label the sample with and

mounting medium. The mounting medium will usually be PBS with thiols added to modulate the blinking frequency as well a Reactive Oxygen Species Scavenging system (ROX). This consists of a mix of enzymes, which deplete the medium of oxygen free radicals. These radicals are the molecules most responsible for photo bleaching since they act as acceptors for the electrons when they are in excited states on the fluorophore electronic system. When the electron is exchanged between the fluorophore and free oxygen, the molecule looses its capacity to fluoresce. Given that in either PALM or dSTORM several thousand images will need to be acquired for a relatively long period, a method to combat bleaching is necessary[3].

Out of the three major super-resolution methods, dSTORM is the easiest to implement on a small budget. The requirements in sample preparation are reasonable enough for a small lab to fulfill. It is also the technique which the highest potential resolution on a regular basis. Therefore, we have set forth to design and implement a dSTORM system that is capable of imaging the SMC complexes in *Drosophila* cells. *Drosophila* cells were chosen for the simplicity of its genome (only 4 chromosomes), the existence of stable cell lines and the possibility to easily establish primary cultures of dividing cells with genetic tags for the proteins of interest. The smaller genome should simplify image interpretation as well as acquisition.

With the establishment of this technique we hope to be able to achieve a better understanding of the structure and function of the SMC complexes, as well as establish a framework to study their interacting partners.

Results

System design and prototypes

In order to develop a Super Resolution system capable of imaging the SMC complexes, and given the simplified hardware requirements for SML microscopy, we first utilized the systems immediately available to us. Organic fluorophores such as Alexa647 have been shown to blink with modest amounts of illuminating power[3]. As such we first tested a Spinning Disk Confocal system (Andor Revolution XD mounted on a Nikon Ti-E with 100x 1.4 objective). To that end, HeLa cells were labeled with antibodies raised against microtubules, secondarily labeled with Cy5 and mounted with the standard ROX buffer. Unfortunately the cells were never visibly blinking (data not shown), possibly due to high-loss of laser light through the spinning disk. The power that reaches the sample from the 50mW 640 nm laser through the 10x objective was roughly 800 μW. The most likely explanation for the lack of observable blinking is that this amount of power was insufficient. There is still the possibility that blinking was still occurring but the background signal of the cells was too high to allow discrimination of single molecules. To further test this, we imaged the cells using a Total Internal Reflection (TIRF) microscope (Roper iLas system mounted on a Nikon Ti-E with a 100x 1.49 objective). TIRF microscopy is a technique which images a small depth (a few hundred nanometers near the coverslip), thereby eliminating out-of-focus background but without the power loss associated with confocal microscopy. The power on this microscope was roughly 250 μW, much less than with the spinning disk. Unsurprisingly, no blinking was observed as well. We therefore concluded that, at least in our hands, super-resolution imaging requires a dedicated microscope.

Commercial super-resolution systems that perform dSTORM have lasers with powers in the range of hundreds of milliWatts. These lasers are prohibitively expensive for a biology laboratory. However, cheaper lasers exist with high power but lower quality specs (for example, elliptical shape and high divergence). These characteristics are acceptable in a dSTORM system since the primary issue is power. With this in mind we acquired an inexpensive laser such as those typically used for show displays. A 639nm laser was available from KVANT s.r.o., ltd in Slovakia, which was more affordable than research laser systems. Considering that the best fluorescent molecules used for super-resolution due to their brightness and blinking characteristics are far-red dyes such as CY5 and Alexa647[3] this laser was chosen for our prototype system. The laser consists of a module with 6 beams packed together to obtain a final 1

W specification (Sup. Fig. 2). For our purposes a single iris in the optical path allowed us to select one of the beams and obtain a single 166 milliWatt beam. With this laser, we adapted a previously existing custom system to image cells with an Hamamatsu Flash 4.0 sCMOS camera and an 63x 1.4 oil immersion objective. This system has the camera and objective in a horizontal configuration, with the sample being held vertically. With this system we made images of S2

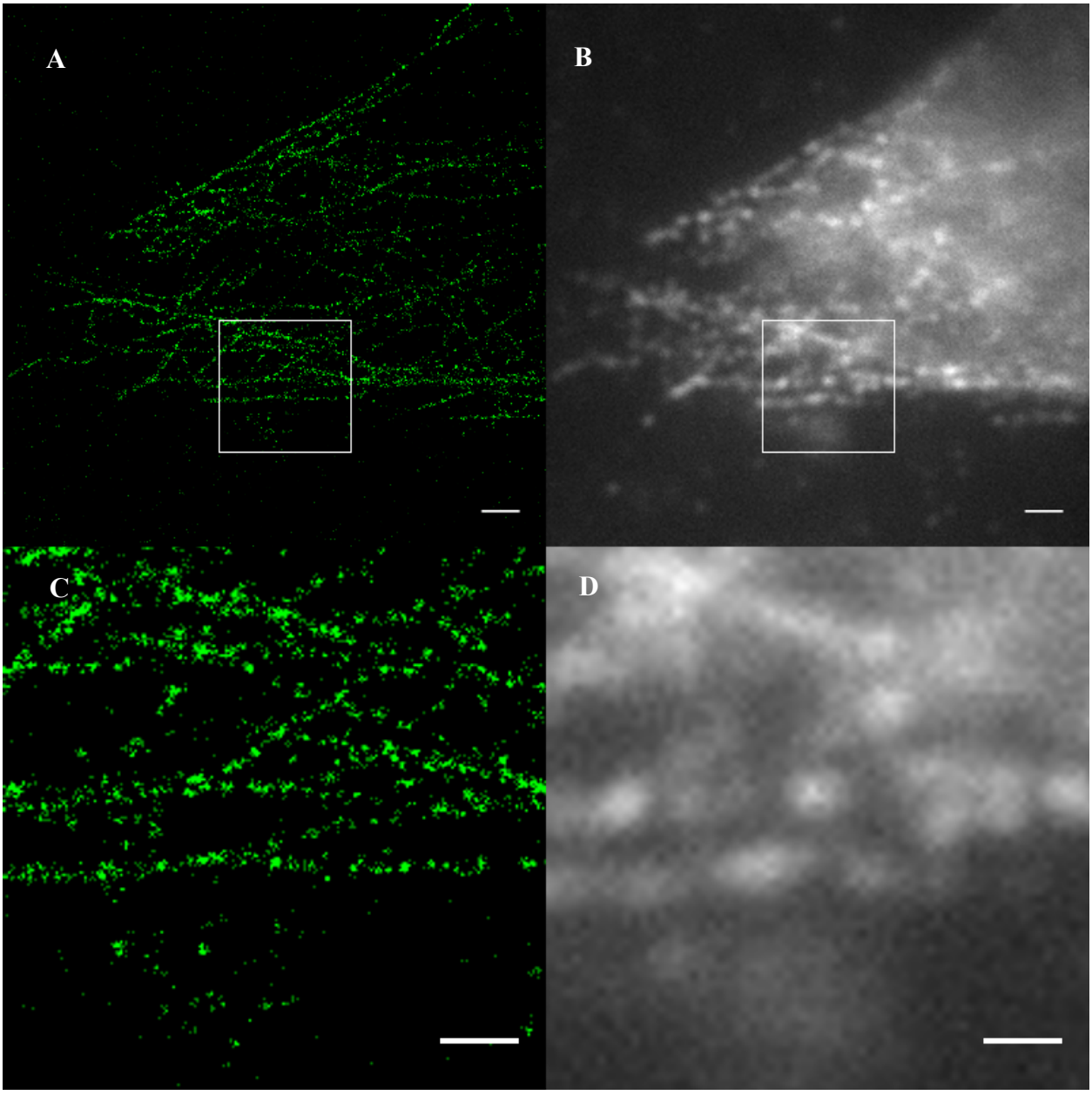

Figure 3 – Super-Resolution imaging of microtubules with the custom system. A - Super-Resolution image and B – Corresponding widefield image; C,D – magnification of the boxed inset in A,B, respectively. Scale bar in A,B is 2 μm and C,D is 1 μm.

cells stained for microtubules and mounted with the ROX buffer and were able to observe the fluorophores entering a dark state and starting to blink (Sup. Fig. 3), which validates our choice of the KVANT laser. Unfortunately, a constant illumination pattern was observed and we presume it was because of problems with aligning the dichroic in a correct manner (Sup. Movie 1). This pattern lowered our collection efficiency. More problematic was the consistent observation of vibrations, which ruined the shape of the image of the single fluorophores. Two other problems were that the sample tended to drift over time in both XY and Z. The XY drift can be corrected by including fiducial markers such as fluorescent beads, but the Z drift was an intractable problem in this microscope. Another issue was the presence of very strong vibrations (Sup. Movie 2). Observing that these vibrations were not always present, we conclude that the problem was not with any part of the microscope and was probably environmental. We speculate that the vibrations were the result of the air conditioning system in the room, whose vibrations were amplified by the vertical sample holder. Such a configuration for the holder might be serving as a lever that amplifies any environmental vibrations. Despite these issues, a few samples were stable enough to have been able to reconstruct an image of the microtubules (Figure 4). In our super-resolution reconstructions, the apparent width of the reconstructed microtubules (see materials and methods) were of about 65±4.5 nanometers (all values mentioned are mean±SEM) average of 30 profiles in four different images). Measuring the width in the widefield images yields a measurement of roughly 480±10.3 nm (average of 15 profiles in three images). Our measurement is then a significant improvement over normal optical resolution but lower than the 30-40 nm that has been reported by others on dSTORM setups with sCMOS cameras[23]. But primarily, the Z drift made the acquisitions very incomplete since insufficient fluorophores were detected.

One possibility to stop the Z drift focus problem would be to stop the acquisition every few frames and run an algorithm that tries to find the plane of focus with the highest intensity to focus again on our sample. This method has the great disadvantage that it greatly extends the imaging time as well as increases the probability that the fluorophores will be bleached away before they are imaged. However, there are commercial systems that solve this problem through hardware. They work by shining infrared light on the sample and measuring the reflection that travels back. The intensity is proportional to the distance to the coverslip, so the system can automatically determine where the coverslip is located and make adjustments to the focus of the

objective so it is constantly at the same distance to the coverslip. This effectively eliminates Z drift, since it is primarily caused by thermal differences between the objective and the stage holding the coverslip[24]. This system is more advantageous than any software solution since it is independent of image acquisition. Most modern automated microscope manufacturers provide this hardware system, such as Nikon's Perfect Focus System (PFS). Because the Nikon Ti-E microscope also has the option of including two dichroic mirror turrets, it becomes fairly easy to insert the KVANT laser on the imaging path of the microscope. With this in mind we were able to acquire a Nikon Ti-E microscope with two dichroic mirror turrets, an Electron Multiplying Charge Coupled Device Andor "iXon Ultra 897" camera and a Nikon 100x 1.45 oil immersion objective. This camera was chosen because it is the most sensitive camera available for low-light level applications. Of these types of cameras it is also the one capable of the fastest exposure

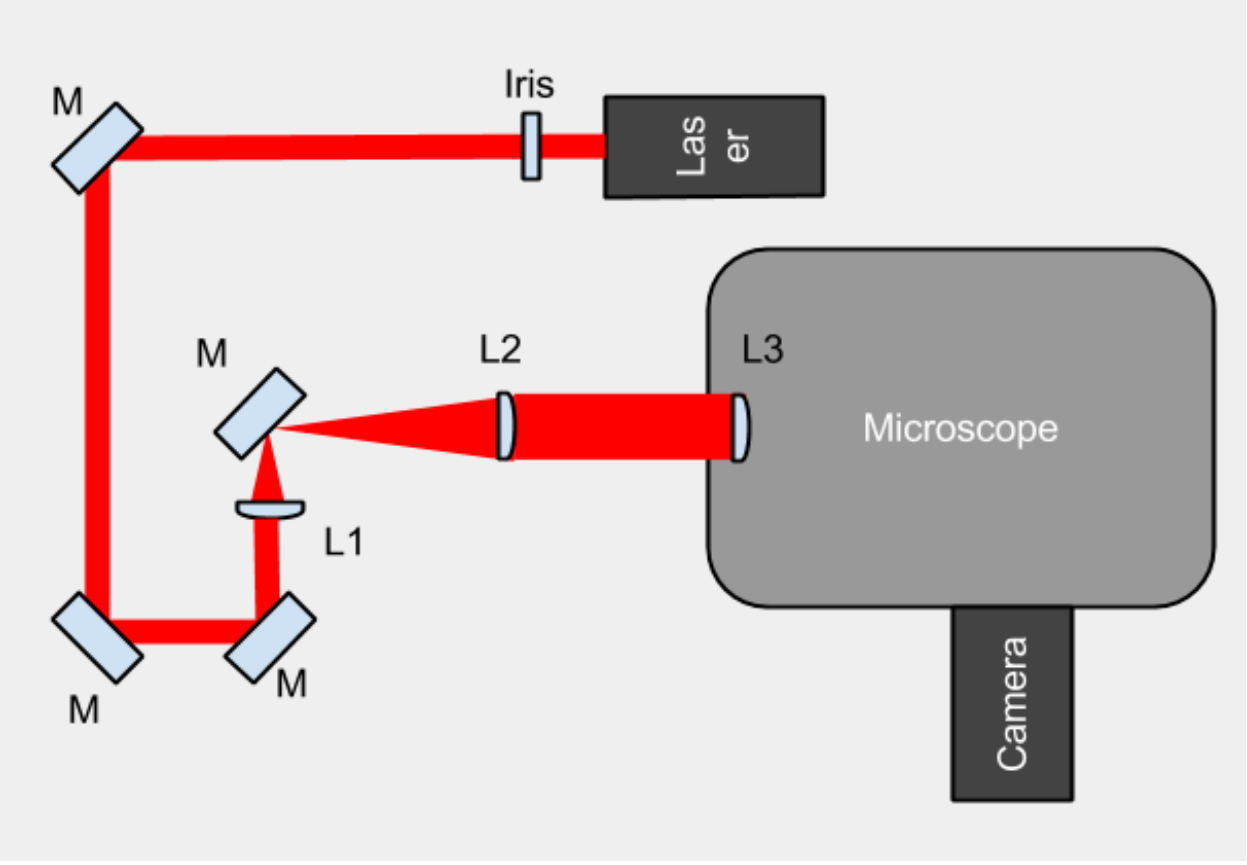

Figure 4 - Schematic layout of the Nikon microscope and KVANT laser system. M – Mirrors; Iris – Iris to filter the unwanted beams from the KVANT laser; L1 – First lens of the beam expander, 10mm focal length; L2 – Second lens of the beam expander, 100mm focal length; L3 – Lens to focus on the back-focal plane of the objective, 200mm focal length. Of note, the placement L2 lens had to be adjusted to correct for the laser's divergence.

times. For SML techniques, these features are important since several thousand frames have to be acquired of relatively dim single molecules. The optical layout to insert the laser on the optical path is described in Figure 5. The beam was raised to the level of the microscope with 2 mirrors, expanded 10x and focused on the back of the objective with an AR coated 200mm focal length lens, which is the tube length advised for Nikon objectives. Had the laser been sent through the objective unchanged it would have been focused into a single point, 100 times smaller, on the focal plane. When focusing on the back focal plane of the objective, an image of the laser fills the field of view, filling the imaged area with laser light.

After aligning the laser and installing the microscope, we could immediately acquire for long periods and the sample was kept in focus for the duration of the acquisitions which varied from 5 to 20 minutes, depending on sample (Sup. Movie 3). With this layout and the fixed positioning of the dichroic mirrors we also did not observe the fixed illumination pattern as with the custom horizontal system. Although there was XY drift present, we could perform super-resolution imaging of S2 cells where the microtubules were immuno-stained with Alexa647 and mounted in ROX buffer (Figure 5). This is only possible after drift correction by including the fiducial markers (see arrow in Figure 6A,B). In our case we used 0.1 μm Tetraspeck beads which are sub-resolution, stable and bright enough for our purposes. To localize and reconstruct the images we used the QuickPALM ImageJ plugin[25] which includes fiducial-based drift correction. Measuring the microtubule width yields a diameter of roughly 72±4 nm, a clear improvement on diffraction-limited conventional microscopy and matching our results with the custom system. Unfortunately our localizations couldn't fully reconstruct a contiguous structure, most likely due to incomplete staining, as other cells seemed to have "broken" microtubules (Figure 5). This could either be the result of incorrect staining or alterations of the microtubule network due to improper sample handling or preparation since they are temperature sensitive. Improper fixation will result in patches like the ones observed. It should, however, be noted that the widefield images look like standard microtubule images and it is only with the super-resolution images that we observe the incomplete structures. Of note, we also did not observe any vibrations detectable by eye. We measured all sub-resolution vibrations present on the system (see Materials and Methods) and could observe mostly contributions from high frequency vibrations (60, 120 Hz) with some lower frequency vibrations (17, 38 Hz), which are normally the result of fan movements (Sup. Fig. 4). These will always be present since the camera and microscope body

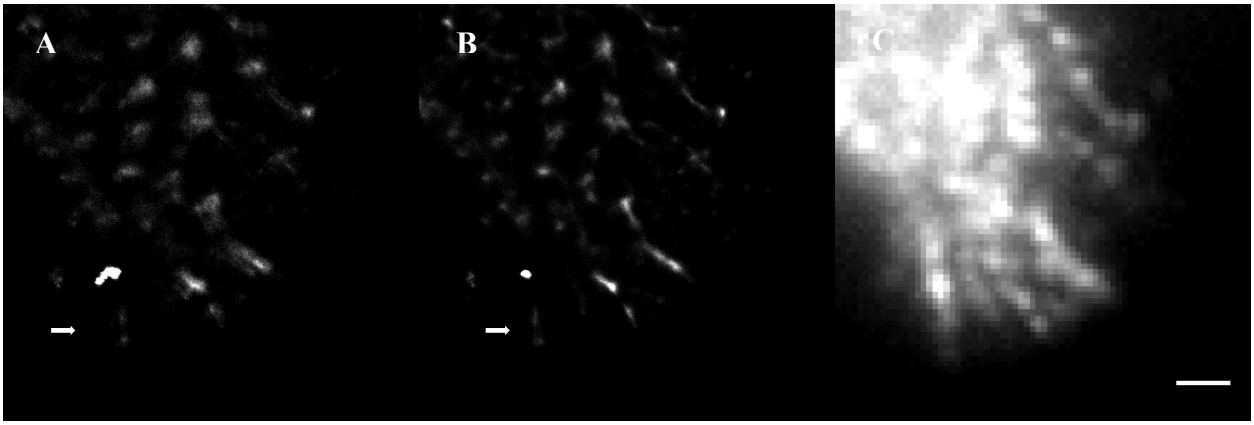

Figure 5 – Microtubules imaged with Super-resolution in the Nikon system. A– Super-Resolution imaging before drift correction and B – after drift correction; A –Widefield image. Arrows point to fiducial marker. Scale bar is 1 μm.

require them for proper functioning and all commercial and homemade systems have them. This means we shouldn't expect them to significantly affect our imaging. Overall, we believe to have implemented a microscope system capable of super-resolution imaging with sufficient resolution to obtain good images of the SMC complexes.

Protocol considerations and optimization

The localization precision in SML super-resolution imaging is dependent on the amount of photons collected and it is this precision which will enable higher resolution images to be obtained[26]. With this in mind, sample preparation for super-resolution imaging has some constraints. One of the first things to care about is to make sure all optical elements are clean. Any particle on the light path will scatter light away and reduce the localization precision. Since the coverslip is part of the optical path, it has to be exceptionally clean and for that we used a very stringent protocol (see materials and methods). Another concern is the reduction of background fluorescence. The total signal collected always has to be above this value, and the higher it is, the lower the total amount of photons can be discriminated. There are many sources for background signal but empirical observation has shown that, in addition to the cells normal background fluorescence, the coating used to adhere cells to coverslips has some auto-fluorescence; the aldehydes used for fixation usually have some inherent fluorescence and mounting media, such as commercial ones, usually possess fluorescent molecules which contribute to the background. The fluorescence of aldehydes is usually in the green wavelengths range, which was less of a concern in our case, given that we were only imaging in the far-red

range. The mounting medium is also usually a source of fluorescence background. When imaging with a widefield microscope, the fluorescence from out-of-focus signals is one of the major contributors to background. Finally, when DAPI is used to stain DNA, the unbound DAPI molecules will still have some fluorescence if not washed away properly[27].

The drawback of the ROX buffer is that it is an aqueous medium. High-numerical aperture objectives, which provide better photon collection, are usually corrected for samples that have a refractive index (RI) matching that of glass (1.51). With samples with a different RI spherical aberration occurs, which severely decreases the resolution and signal obtained the deeper one images. The RI of the medium is also a limiting factor in collection efficiency because the effective numerical aperture of the system will be limited to the RI of the sample's medium. This means that if we image a sample that is in water, whose RI is 1.33, with a 1.45 NA objective the resolution and signal of the image will be as if it had been captured with a 1.33 NA objective. With fixed samples, glycerol based mounting media are usually used, to obtain a higher RI since the RI of glycerol is 1.47. During our optimization of the protocols for dSTORM imaging of the SMC complexes, Olivier et al. demonstrated that the commercial mounting medium Vectashield is capable of inducing blinking in some dyes for dSTORM[28], such as Cy5 and Alexa647. Vectashield has higher auto-fluorescence than ROX buffers, but it also has an RI of 1.44 which means that greater photon collection can be achieved than with water-based media. Taking these two into account, Vectashield outperforms the ROX buffers for dSTORM imaging[28]. Importantly, Vectashield is non-toxic in contrast to the ROX buffer because of the presence of β-mercaptoethanol. Therefore, Vectashield which does not include DAPI in its formulation was selected as the preferable mounting medium and unless stated otherwise it was used throughout this study.

In addition to the most adequate mounting medium, super-resolution imaging also benefits tremendously from a flat sample preparation as it will reduce the distance to the coverslip (and therefore spherical aberration) as well as reduce the out-of-focus fluorescence. Both of these factors affect tremendously the quality of the signal collected for each molecule and in turn, the final resolution of the Super-Resolution image. Cells prepared for normal fluorescence are usually grown on coverslips coated with some sort of molecule to promote adhesion and will have a certain thickness. For Super-Resolution imaging we set out to obtain cells that were flat, very close to the coverslip and did not require the use of adhesion molecules

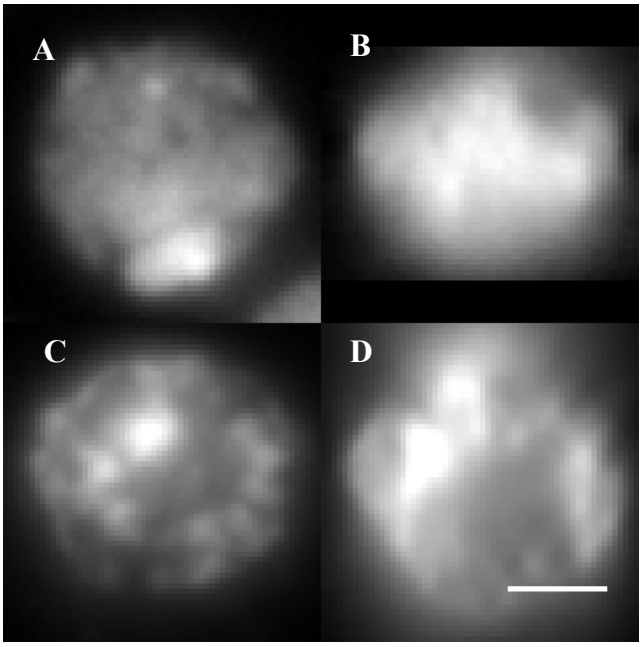

Figure 6 – Widefield microscopy of S2 cells prepared by Cytospin (A) or grown on concanavalin (C) and their respective XZ projections (B, D) Scale bar is 2 μm.

(as these can also increase the background fluorescence). To that end, we optimized a protocol using a Cytospin centrifuge (see materials and methods). Briefly, the Cytospin is a centrifuge with spacers to hold microscopy slides and holders to receive cells in suspension. When the centrifuge starts rotation, the cells escape their holder at high speed and hit the slide with enough strength to become attached and flat. For super-resolution imaging we attached coverslips onto slides and centered them on the area where the cells were expected to hit. In this way, we could obtain flat cells adhered to coverslips, with low background (Figure 6). By immersing the cells in a hypotonic solution and performing Cytospin, the cells burst on contact with the coverslip and mitotic cells spread their chromosomes in a manner that enables us to distinguish single chromosomes. To enrich the cell suspension for dividing cells we incubate with colchicine, a microtubule depolymerizing agent, which arrests cell division.

One issue that is specific to dSTORM imaging is the effect of antibody-stripping, ie the removal of fluorophore binding to antibodies due to the presence of large amounts of laser light. This results in several spots being observed with Brownian motion which can be identified incorrectly and cause artifacts in the reconstruction as well as diminish the amount of fluorophores which can be localized. To solve this, a second fixation step after the immuno-staining was included, simultaneous with DAPI incubation. After washing the formaldehyde and DAPI away, Tetraspeck beads were added to the preparations to serve as fiducial markers. These beads are normally in solution when diluted in water but tend to adhere to the coverslip glass when diluted in PBS.

Super-resolution imaging and reconstruction

Before attempting to image the SMC complexes, which are not easy to perform immuno-staining on, a staining against other proteins with a known and identifiable structure should be used to validate the system. To that end we have first performed staining against microtubules. Microtubules are hollow cylindrical structures with a width of roughly 25 nanometers on the outer diameter and 12 nm on the inner diameter, as determined by TEM[29]. They serve as a good validation of super-resolution systems, in both their ability to properly recover a structure and in measuring the resolution that is achieved with the method or system being tested. Our first custom system was able to achieve a reconstruction where the microtubules had an apparent width of 65 ±4.5 nm (Figure 3) but the measurements made with the Nikon microscope gave us a size of roughly 72 ±4 nm (Figure 5), with a moderate recovery of the structures visible in widefield microscopy. This recovered size is a 6 fold improvement on the 480 nm width measured in our widefield images and is getting closer to being able to resolve the 25nm width of the structures. The structures were patchy, but this could be a result of our fixation protocol and not the imaging itself.

Microtubules are located in the cytoplasm, which makes them more accessible than nuclear proteins. In order to be able to stain nuclear proteins, a strong extraction step is required simultaneous with the fixation, in contrast with the microtubules, which require that the detergent extraction step be performed after fixation, or they will destabilize before the formaldehyde can act. Hence, we changed our protocol according to the target protein (see Materials and Methods). As well, the chromatin is a very densely populated area of the cell and in its very center. This makes staining for nuclear proteins more difficult than cytoplasmic proteins and structures. Before moving to imaging the SMC complexes and to validate a protocol

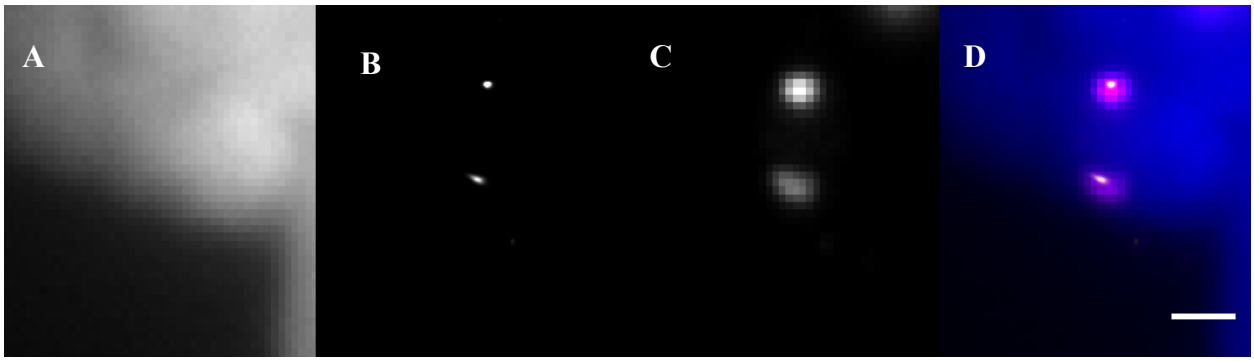

Figure 7 - Super-Resolution reconstruction of CENPC stainings in interphase S2 cells grown in Concanavalin A. A - Widefield DAPI; B - Super-resolution image; C – Widefield image of CENPC; D - Merge. Scale bar is 1 µm.

that can permit super-resolution imaging of nuclear proteins as well as the imaging system itself, we have performed immuno-stainings against CENPC or Cid. These are two proteins that locate to the centromeres of mitotic chromosomes[30]. EM imaging of kinetochores of metaphase S2 cells with attached microtubules (which are stretched, and therefore, bigger) has shown their size to be around 40 to 50 nm[31]. Imaging interphase S2 cells with our Nikon system (Figure 8) has afforded us to reconstruct the centromere complex with an apparent width of 76±2.96 nm (average of 41 profiles). This is in stark contrast to the 360±7.5 nm measured in our widefield images (average of 10 profiles in 3 images). While we are still not fully resolving the complex, this is a clear improvement on the widefield imaging, and it very nearly reaches the width measured with TEM. This made us confident in our capability to be able to image the SMC complexes with super-resolution.

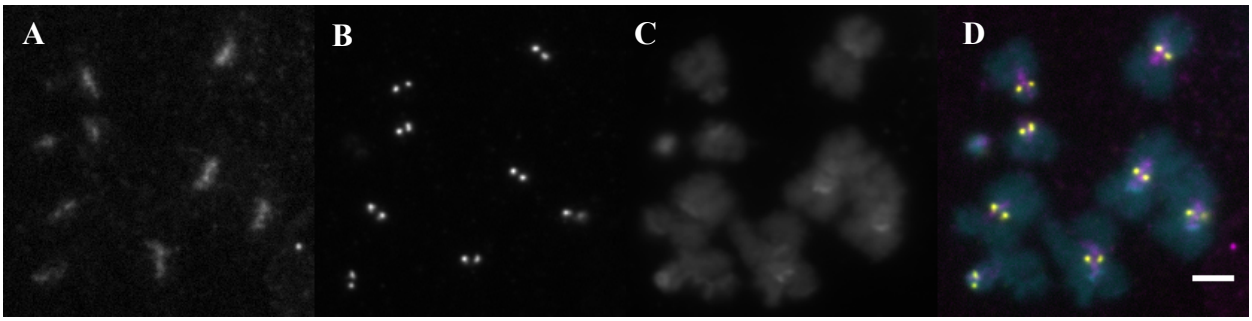

Figure 9 – Rad21 stained S2 cells prepared by Cytospin. A – Rad21 with Alexa647; B – CENPC with FITC; C – DAPI; D – Merge. Scale bar is 2 µm.

In order to image the cohesin complexes we performed immuno-stainings against R*ad21*, the *Drosophila melanogaster* homolog of Scc1, which is the kleisin subunit of the cohesin complex (Figure 9). Observing chromosome spreads of S2 cells stained for both Rad21 and CENPC shows the typical pericentromeric distribution of cohesin in mitotic cells. Performing super-resolution reconstruction allows us to observe a more restricted localization of the Rad21

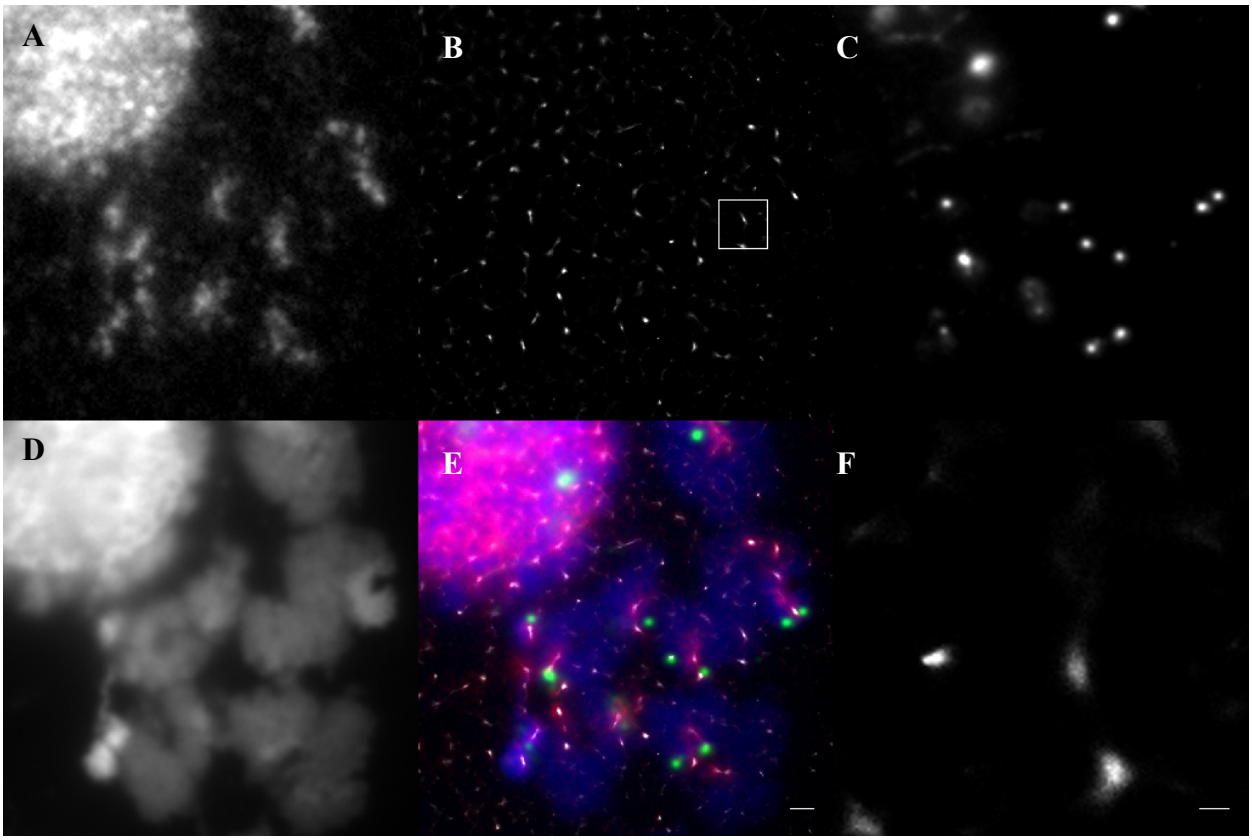

Figure 10 - Super-Resolution reconstruction of Cohesin. A – Widefield image of Rad21 with Alexa647; B – Super-Resolution reconstruction of A; C – CENPC with FITC; D – DAPI; E – Merge; F – Magnification of boxed inset in B. Scale bar in E is 2 µm and 200 nm in F.

protein, with a width of roughly 87±2.9nm (average of 45 profiles over 5 images; Figure 10f). To compare, the widefield images gave a width of roughly 460±12.9 nm (average of 14 profiles over 4 samples). These results require further optimization and validation as several structures could be detected also outside the chromosomes, structures that were otherwise not observable with conventional microscopy images of Rad21 (Figure 10b), which suggests that they result from artifacts specific to dSTORM imaging. When analyzing the raw image stack we can observe several overlapping points in the initial frames as well as more blinking outside the chromosome regions than would be expected. Despite this, we have been able to reconstruct the region that corresponds to the Rad21 labeling with super-resolution. Initial observations would indicate that the cohesin complex seems restricted to a thin axial structure restricted to the middle of the chromosome.

We have attempted to perform a similar analysis on condensin complexes, to evaluate whether the central axis organized by condensins would be also a thin structure in the 80 nm range. However, due to problems with the specific antibodies we could never get the immunostaining to work (see Sup. Fig. 5). We performed immuno-stainings against *Barren*, the *Drosophila melanogaster* homolog of CAP-H, which is the non-SMC subunit of the condensins, as well as SMC4. We attempted to use different secondary antibodies, different concentrations of the primary antibody and incubating overnight instead of during 1h, but could never detect staining. Staining simultaneously with Cid or CENPC always worked, which controlled for experimental errors. As previous work has shown that condensin antibodies work nicely using similar protocols in *Drosophila* tissue culture cells[32] we assume that the antibodies used here were no longer in proper condition. Nevertheless, given the favorable initial results for Rad21-EGFP, we expect that similar analysis can be performed for condensins once better antibodies become available. In addition, as flies carrying Barren-GFP constructs have also been produced[12], super-resolution of cells derived from fly tissues may also be possible in the future.

Discussion

Overall, we feel confident that we have established a reliable system capable of producing super-resolved images of the SMC complexes, as well as of other molecules of interest. Using standard antibodies and cultured *Drosophila* cells we have been able to reconstruct super-resolution images of the Rad21 cohesin subunit. Although still preliminary, our results suggest that cohesin complexes are holding sister chromatids solely at the most inner part of the mitotic chromosomes, in a region of under 90 nm. This, as far as we are aware, is a new result. Although previous widefield imaging also showed localization in the inner axis of the chromosome, the resolution of widefield microscopes prevented further clarification as to the actual distribution of the localization. Would cohesin be spread around the width of the chromosome? Does it have a speckled distribution or does it correspond to a tight, dense area? Our preliminary results show a tight localization in the inner axis of the chromosome. A tight axial localization could diminish the probability of catenation occurring between the sister-chromatids as it means the chromosomes are very well separated from each other, helping to prevent missegregation errors. Catenation would be far more likely to occur if the cohesin complexes were distributed around the entire width of the chromosome, as it would imply the DNA of both chromatids would have to locate in regions of inevitable overlap. Our results start to draw an image of the chromatids as being restricted to defined spatial domains of the overall chromosome structure.

The interaction of each cohesin complex with DNA is speculated to fall either under a "strong" or "weak" model and our method could help shed some light on this question. The weak models hold that the each ring holds only one DNA strand and they interact (either topologically or through a mediator, like the Scc3 protein[33]) with another cohesin ring holding the sister strand (Figure 2b,c). There is very little evidence that a mediator is holding the rings and there is some strong biochemical data indicating that this is not the case[6]. It is possible that two rings hold each other topologically (Figure 2b). If we postulate that the Cohesin rings are distributed in a planar arrangement that separates the sisters in two domains, we would expect to consistently find localizations in a region over 100 nm wide (Figure 11b). This value is based on the proposed notion that the rings can rotate and that there is no constraint on the ring orientation, and there is some evidence that the rings have some freedom of movement[6] (Figure 11a,c). The estimate of a

value greater than 100 nm is due to the 50 nm length of each of the two rings, plus the 20-30 nm added by the use of a primary and a secondary antibody. If we consider that there should be hundreds of cohesin molecules on a given region, the overall size of the region should average into the 100 nm estimated value. Admittedly, 13% of our measurements of Rad21, the *Drosophila* homolog of Scc1, reached 100nm. However, the majority of our localizations are restricted to a region of around 80 nm. As yet, we have very few measurements and require more to be more certain of our measurement. Nonetheless, we believe our preliminary estimate of 87±2.9 nm, if confirmed, presents a major argument against this model. On the other hand, the strong model proposes that each ring holds a DNA strand as well as its sister strand (Figure 2a). Under this model, and again assuming a linear arrangement along with free rotation of the rings, we would expect the localizations to occupy a region of at least 50 nm, plus the 20-30 nm introduced by the antibodies (Figure 11a). Strikingly, our results show that the Rad21 subunit of the rings localize to a ~85 nm wide axially defined region. This value is remarkably similar to what one would expect under the strong model.

These results raise the question of the relative localization of the remaining partners of the SMC complexes. In the weak model where the ring complexes are bound to each other through Scc3, one could speculate that the localizations of Scc3 would follow a similar but more restricted axial profile while the hinge domains would spread further out. If Scc1/Rad21 is interacting with Scc3, then its localizations would closely follow Scc3 and would have a very restricted localization profile, not dissimilar from what we observe (Figure 11b). But if the rings are only interacting topologically, then we shouldn't expect Scc3 or Scc1 to have different localizations from SMC1/3 unless the rings are forced into a specific configuration (Figure 11c). As for the strong model, it predicts a more restricted axial localization of all partners than if the two rings are bound together topologically (Figure a,c). Going forward, if one could simultaneously image the several proteins involved in the complexes, one could help further clarify which of the models is valid.

Our result of 87±2.9 nm could still simply correspond to the resolution that we obtained with our system, as it is very similar to the values obtained with microtubules (72 nm) and centromeres (65 nm). If we are still limited in resolution, and the localization is further restricted into an axial domain of perhaps a few tens of nanometers, this would provide further insight into the structure of the chromosome itself as two spatially defined chromatids, as well as to start

pointing towards validating a weak or strong model as the above mentioned experiments mention. The question then arises: what resolution are we achieving with each image? The width of the apparent structures is a good indicator, if the size of that structure is known (such as

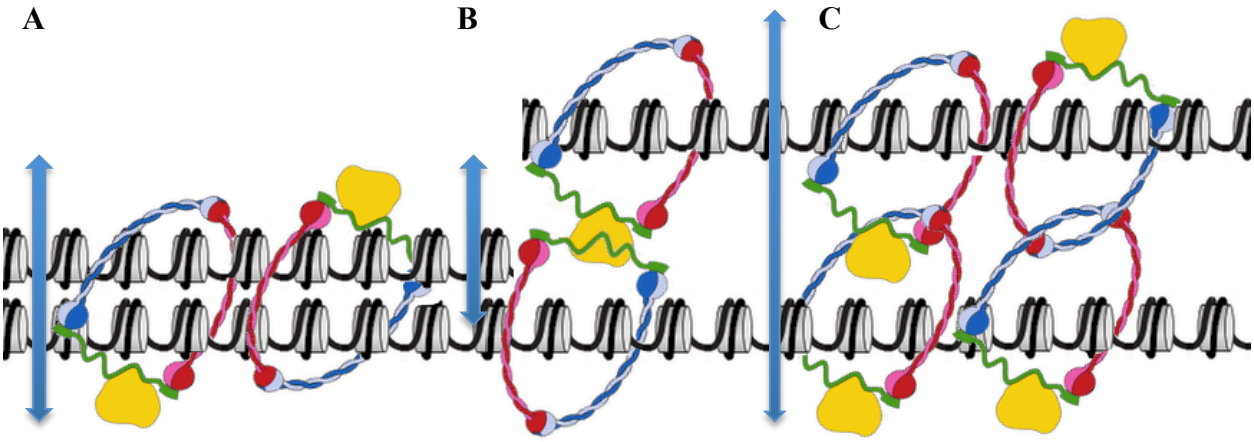

Figure 11 – Explanatory models for possible localizations of the cohesin complexes. A – The strong model proposes that a single ring embraces both strands, limiting the possible localizations to a 50nm region but with every subunit distributing themselves randomly; B – One of the weak models proposes that Scc3 (in yellow) links both rings, which would stabilize thes possible localizations of each subunit to a specific área; C – If both rings are topologically bound, any subunit could be located anywhere in a region of 100nm.

the case of the centromeres and microtubules). In the future, simultaneous imaging of centromeres with the SMC's might serve as an internal resolution measurement for the capabilities of the hardware. If the width of both structures is similar and still above the 40 to 50 nanometers expected of the centromere, then we are still not resolving the structure completely and it is probably more restricted than we realize currently.

As mentioned before, the observed localization of the complexes is confounded by the use of a secondary amplification system, where an antibody binds to another antibody. These have a size of roughly 10 to 15 nanometers[5] and will have several of the secondary antibodies binding to the primary antibody. This will increase the size of the measured structure. This issue not usually a problem with widefield imaging as the error this introduces is below the resolution of the microscope. To alleviate this issue, Ries et al. performed super-resolution imaging using nanobodies[4]. These are antibody fragments where only the part of the antibody which is selective to the target protein is used in the staining and are roughly 1.5 to 2.5nm in length[34]. This

nanobody will have an organic fluorophore directly attached to it, which is smaller than 1 nm. As a generalist approach, a nanobody against GFP is a very versatile tool since there are many existing strains tagged with GFP and the GFP molecule is roughly 4nm long[35]. It is also highly specific, which should reduce labeling artifacts. Immuno-staining of the cohesin complexes using nanobodies targeting GFP should be feasible in *Drosophila*, as our laboratory has recently established Drosophila stocks carrying GFP-tagged Rad21 in a mutant background[36]. As such, cells derived from rescued stocks in which all Rad21 subunits are labeled with GFP should be a good source to perform these experiments. Given the vast amount of fly strains with GFP tagged proteins available, super-resolution images could also be obtained for other protein partners who interact with the SMC complexes with relative ease.

The use of flies instead of transfected cell lines has the added advantage of providing us with several cell types and developmental stages to investigate the process in different contexts. The *Drosophila* brain, for example, has many dividing cells and many protocols have been developed to image the cells. For super-resolution imaging, as mentioned before, we would like to have the thinnest sample possible. With that in mind, we have made initial attempts to optimize sample preparation of primary cultures of cells derived from Drosophila larval. These attempts have mostly failed due insufficient recovery of chromosome spreads. Successful metaphase spreads are the result of a hypotonic shock that is strong enough to disrupt the cell, but not strong enough as to distort chromosome morphology. Varying the salt concentration or the time of exposure to the hypotonic solution, with timing being the hardest step to control, can modulate this. Unfortunately some variability will be present since the time from re-suspending in the solution and placing the suspension on the cytospin machine will depend on the operator's speed in pipetting and the number of slides to prepare. Other solutions in other model systems used for the hypotonic shock have slower exposure times and might provide more consistent results. Another point is that classical chromosome spread protocols involve a Methanol and Acetic Acid fixation step before the cytospin or drop technique step. These techniques are not so amenable to immuno-fluorescence and a formaldehyde fixation is preferable. Perhaps fixing the cells in suspension in formaldehyde, shocking and performing the cytospin could provide better results, but the formaldehyde crosslinking might also prevent decent spreading of the chromosomes. However, we envision this should be feasible in the near future through further optimization.

Another technique is tissue squashing, where the tissue (such as larval brains) is pressed between a slide and a coverslip in order to adhere to the coverslip. If treated with colchicine, the brains will have several chromosome spreads visible. Unfortunately the resulting sample is usually thicker than what is obtained with cytospin. The thickness would result in samples where spherical aberration would be an issue with oil objectives and scattering of light would be significant. Water immersion objectives could be used for ROX buffer mounted samples, but would limit the amount of photons that could be collected, given their lower NAs. The use of Vectashield reduces the spherical aberration considerably however, and perhaps one could attempt super-resolution imaging of brain squashes mounted in Vectashield. To note, scattering would still be a problem. In order to diminish this scattering, there are methods which make samples transparent and change their refractive index to that of glass[37], so called clearing techniques. However, such samples don't reflect any light and the Perfect Focus System used to maintain the samples in focus would no longer function properly. Building a system which is thermally well isolated, or where the objective and stage are fused together and made of the same materials, preventing thermal focus drift, could solve this. Another option would be to have a system where drift is corrected in real-time by the use of fiducial markers that would be imaged by a separate system.

In addition to the imaging of cohesin complexes, this project aimed at the super-resolution imaging of the related condensin complexes. However, due to technical difficulties, we were unable to successfully accomplish this. Most of the problems were related to quality of antibodies, a problem that can be circumvented in the near future by the use of new antibodies or staining cells from Barren-GFP fly stocks, which are present in the lab, with nanobodies that target GFP. Unfortunately that was not possible within the time frame of this project, but we believe that the nanobodies are the best step forward.

Of great interest would be to obtain images of the SMC complexes in the DNA context. To that end, one would like to image DNA structures with greater resolution as well. A few techniques have been used for DNA imaging, namely imaging of genetically tagged-histones[38], using organic fluorophores tagged to dUTP[39], with FISH probes[40] and with DNA intercalating dyes[41]. DNA intercalating dyes are promising since they are relatively simple to implement and have a small size. They are limited in their quantum yield and absorption cross-section, however, and would provide limited localization precision compared to the use of organic fluorophores

like Alexa647. The use of dUTP tagged with organic fluorophores would permit super-resolution imaging with good collection efficiency and requires only a commercially available kit. It can only image limited stretches of DNA as opposed to the entire structure, but given the density of the DNA in the nucleus, this could be beneficial to imaging and interpretation. Adding more lasers to our current system would enable multicolor imaging, and therefore, imaging the SMC complexes in their chromosomal context.

With regards to density, mitotic chromosomes are tightly packed, which should make staining more difficult. In this work we focused on imaging mitotic chromosomes since the structural differences inherent to the chromosomes are more readily interpreted. During the imaging of mitotic chromosomes, however, some interphase nuclei were also present in the field of view. Some structure is observed inside these but these structures are similar to those seen outside the nucleus, which we expect to be staining artifacts. In the observed interphase nuclei we expected to see long, linear structures, which would correspond to the backbone of the chromosomes. But we only see short, discontinuous structures (Figure 10f). These could be artifacts, the result of secondary antibody aggregation and not of actual cohesin staining. If the acquisition and staining protocols are improved to eliminate the artifacts outside the cells fully, and these structures can still be detected and reconstructed we can be sure that we are resolving the interphase distribution of Rad21. One explanation for seeing only short stretches is that the three dimensional distribution of the DNA would bring the linear structure in and out of focus, but this is unlikely in cytospin preparations given that the nucleus is flattened to be almost entirely in focus. Another hypothesis is that the staining is incomplete for the most part. This could be because the antibody didn't have access to the cohesin protein to bind in heterochromatic stretches. However, the mitotic chromosome is much more tightly packed and we can see the pericentromeric structure. The observed structure could still be the result of only parts of the cohesin distribution that are easily accessible. The tight packing of the nucleus could also be scattering the light emitted by the stained areas. Perhaps imaging cleared samples will improve collection enough to discriminate cohesin structures. With cleared samples, thicker specimens can be used which might alleviate the packing somewhat. With such samples one could attempt to image in three dimensions with the simple addition of a cylindrical lens to the microscope, as with the QuickPALM system[25]. By 3D imaging a dUTP staining of DNA and

cohesin, one could help clarify which of the current models for cohesin and condensin interaction with DNA is more likely[42].

In summary, we have here described a system and set of protocols that is already capable of resolving the localization of the cohesin complexes to an axially restricted area of the chromosome. Although further optimization of the protocols is still required, we believe we will soon be capable of imaging the condensin complexes as well. Imaging the SMC complexes and its partners with greater resolution will help expand our knowledge of the dynamics of chromosome behavior and structure. With further expansion of the hardware by adding lasers, the creation of protocols which can harness the power of nanobodies and by improving super-resolution capable mountants, we can go further than the results presented here and create a super-resolution map of not only the primary players involved in the structure of the mitotic chromosome, but the interphase nucleus as well.

Materials and methods

Microscopy systems

Most images were acquired on the Nikon setup described above. Briefly, a Nikon Ti-Eclipse motorized microscope equipped with an Andor "iXon Ultra 897" camera, a KVANT s.r.o. 1W laser and a Nikon 100x Plan Apo lambda 1.45 objective were used to obtain all images shown. In order to obtain clear images we remove any scattering particles. To that end, coverslips and slides were cleaned by immersion in acetone, then methanol, and washed 3 times in ultrapure water, repeating the entire procedure 3 times. A final 30 minute incubation in KOH in a sonicator water bath was followed by washing with ultrapure water. Coverslips were stored in the ultrapure water until needed, at which time they were air-dried inside a flow-hood or incubated for 10 min with 0.5mg/ml Concanavalin A (Sigma Aldrich). Coated coverslips were dried in the flow-hood with the UV lamp turned on. For super-resolution imaging, only coverslips with low tolerance for thickness deviation (Zeiss, 474030-9020-000) were used in order to diminish any spherical aberration.

Chromosome spreads

In order to obtain chromosome spreads, S2 cells were incubated in 30 μM colchicine for 5 hours. S2 cells were centrifuged for 1 minute at 3000 rpm, were then re-suspended in a 0.5% solution of sodium (Sigma Aldrich, W302600) and placed in a Cytospin machine (Wescor Cytopro 7620 cytocentrifuge). Cells were then centrifuged for 1800 rpm for 5 min unto either slides or coverslips, as noted. Cell re-suspensions were made as briefly as possible, unless noted.

Immunostainings

Cells to be immunostained were centrifuged in a cytospin machine or grown in Concanavalin A coated coverslips, as noted. Cells were washed in PBS and then fixed for 10 min by incubating in 3.7% formaldehyde (100 μl of 37% formaldehyde solution (Sigma Aldrich, 47608) diluted in 900 μl of PBS with 0.5% Triton-X100 (Sigma Aldrich, X100), except when staining for microtubules. In that case, they were fixed in 4% formaldehyde diluted in PBS followed by a 10min incubation in PBS with 0.5% Triton-X. They were washed three times for

5mi in PBST (PBS with 0.05% Tween 20 (Sigma Aldrich, P7949)). Next, they were immuno-blocked for 30min in block (10% fetal bovine serum diluted in PBST). It was followed with incubating with the primary antibody diluted in block solution (Guinea pig anti-Rad21[43], 1/500; Rabbit anti-CENPC[44] 1/5000; Rat anti-Cid, 1/1000 (gift from C. Sunkel); Mouse anti-α-Tubulin (DM1A, Sigma) 1/4000; Rabbit anti-Barren[45] 1/500; Rabbit anti-DmSMC4[46] 1/500). They were then washed three times for 5min in PBST and then incubated for 45min with the secondary antibodies diluted 1/500 (unless noted) in block solution. After three washes of 5 min each with PBT, the cells were fixed again with 4% formaldehyde diluted in PBST and with DAPI (Cell Signaling Technology, 4083S, final dilution of 10000x), unless otherwise noted. After, Tetraspeck beads (Life Technologies, #T-7279) which were previously diluted 10 x in ultra-pure water were added in 1µl drops onto the PBST covered slides or coverslips and left standing for 30 min.

Sample mounting

For super-resolution imaging with the reactive oxygen species buffer (ROX buffer), a solution is first prepared with 400 µg/mL Catalase (Sigma Aldrich, C1345), 1% β-Mercaptoethanol (Sigma Aldrich, M6250), 500 µg/mL Glucose Oxidase (Sigma Aldrich, G7141) diluted in PBS. This was stored for up to four months. On the day of imaging, a 1ml aliquot was taken and had 10 mg of glucose added to it (Sigma Aldrich, G8270). The slides were covered with parafilm and heated to 70ºC to melt the parafilm. After cooling down, a small square of roughly ~1cm^2 was covered in order to create a chamber with sufficient buffer to image the cells. Roughly 20 µl of buffer was placed on this square and the coverslip was placed on top, with the cell side facing the slide (Sup. Fig.). The surface of the mounted coverslip was dried in order to then seal the slide with nail-polish ("Lovely Girl" brand clear nail-polish). Vectashield (Vector Labs, H-1000) mounted slides were mounted by placing a 5 µl drop of the medium on a slide, placing the coverslip with the cell side facing the slide on top, removing excess liquid and then sealing with nail-polish.

Image analysis and reconstruction

All image acquisition on the Super-Resolution, SPIM and Andor systems were made with the Micro-Manager open source software[47]. Acquisition on the Roper TIRF system was done with the MetaMorph software package (Molecular Devices). All image analysis was made with

the most up-to-date version of FIJI, an analysis package of the ImageJ open source software[48] which included the QuickPALM super-resolution localization and reconstruction plugin[25] used for all reconstructions in this work.

The apparent width of structures was measured using the standard ImageJ tools by measuring the width of the profile of a given structure at values which corresponded to half the maximum after background subtraction.

Vibration measurements

Vibrations were measured in the system by acquiring at 331 frames per second a cropped region of the chip where a static Tetraspeck bead was being imaged. Using FIJI, the resulting stack was background subtracted and for each frame, the bead was located. Finally, the displacement of the bead on each frame to the original frame was plotted. We calculated the one dimensional Fast Fourier Transform to obtain the frequencies present in the vibrations using the calculator provided in the website in reference [49].

References

1. Wood, A. J., Severson, A. F. & Meyer, B. J. Condensin and cohesin complexity: the expanding repertoire of functions. *Nat. Rev. Genet.* **11,** 391–404 (2010).
2. Henriques, R. & Mhlanga, M. M. PALM and STORM: what hides beyond the Rayleigh limit? *Biotechnol. J.* **4,** 846–57 (2009).
3. Van de Linde, S. *et al.* Direct stochastic optical reconstruction microscopy with standard fluorescent probes. *Nat. Protoc.* **6,** 991–1009 (2011).
4. Ries, J., Kaplan, C., Platonova, E., Eghlidi, H. & Ewers, H. A simple, versatile method for GFP-based super-resolution microscopy via nanobodies. *Nat. Methods* **9,** 582–4 (2012).
5. Sarma, V. R., Silverton, E. W., Davies, D. R. & Terry, W. D. The three-dimensional structure at 6 A resolution of a human gamma Gl immunoglobulin molecule. *J. Biol. Chem.* **246,** 3753–9 (1971).
6. Nasmyth, K. & Haering, C. H. Cohesin: its roles and mechanisms. *Annu. Rev. Genet.* **43,** 525–58 (2009).
7. Oliveira, R. A. & Nasmyth, K. Getting through anaphase: splitting the sisters and beyond. *Biochem. Soc. Trans.* **38,** 1639–44 (2010).
8. Cuylen, S. & Haering, C. H. Deciphering condensin action during chromosome segregation. *Trends Cell Biol.* **21,** 552–9 (2011).
9. Pauli, A. *et al.* Cell-type-specific TEV protease cleavage reveals cohesin functions in Drosophila neurons. *Dev. Cell* **14,** 239–51 (2008).
10. Haering, C. H., Farcas, A.-M., Arumugam, P., Metson, J. & Nasmyth, K. The cohesin ring concatenates sister DNA molecules. *Nature* **454,** 297–301 (2008).
11. Earnshaw, W. C. & Laemmli, U. K. Architecture of metaphase chromosomes and chromosome scaffolds. *J. Cell Biol.* **96,** 84–93 (1983).
12. Oliveira, R. a, Heidmann, S. & Sunkel, C. E. Condensin I binds chromatin early in prophase and displays a highly dynamic association with Drosophila mitotic chromosomes. *Chromosoma* **116,** 259–74 (2007).
13. Gerlich, D., Hirota, T., Koch, B., Peters, J.-M. & Ellenberg, J. Condensin I Stabilizes Chromosomes Mechanically through a Dynamic Interaction in Live Cells. *Curr. Biol.* **16,** 333–344 (2006).
14. Bendersky, L. A. & Gayle, W. Electron Diffraction Using Transmission Electron Microscopy. *J. Res. Natl. Inst. Stand. Technol.* **106,** 997–1012 (2001).
15. Grimaldi, F. M. *Physico-mathesis de lvmine, coloribvs, et iride, aliisque adnexis libri duo: opvs posthvmvm*. (Bononiae, 1665).
16. Abbe, E. Beiträge zur Theorie des Mikroskops und der mikroskopischen Wahrnehmung. *Arch. für Mikroskopische Anat.* **9,** 413–418 (1873).
17. Cox, G. *Optical Imaging Techniques in Cell Biology, Second Edition*. 316 (CRC Press, 2010).

18. Rose, H. H. Optics of high-performance electron microscopes. *Sci. Technol. Adv. Mater.* **9,** 014107 (2008).

19. Girit, C. O. *et al.* Graphene at the edge: stability and dynamics. *Science* **323,** 1705–8 (2009).

20. Schermelleh, L., Heintzmann, R. & Leonhardt, H. A guide to super-resolution fluorescence microscopy. *J. Cell Biol.* **190,** 165–175 (2010).

21. Schüttpelz, M., Wolter, S., van de Linde, S., Heilemann, M. & Sauer, M. dSTORM: real-time subdiffraction-resolution fluorescence imaging with organic fluorophores. **7571,** 75710V–75710V–7 (2010).

22. Henriques, R., Griffiths, C., Hesper Rego, E. & Mhlanga, M. M. PALM and STORM: Unlocking live-cell super-resolution. *Biopolymers* **95,** 322–331 (2011).

23. Huang, F. *et al.* Video-rate nanoscopy using sCMOS camera-specific single-molecule localization algorithms. *Nat. Methods* 1–9 (2013). doi:10.1038/nmeth.2488

24. Peters, J. Nikon Instruments TiE-PFS Dynamic Focusing System. *Nat. Methods | Appl. Notes* (2008). doi:10.1038/an6676

25. Henriques, R. *et al.* QuickPALM: 3D real-time photoactivation nanoscopy image processing in ImageJ. *Nat. Methods* **7,** 339–340 (2010).

26. Thompson, R. E., Larson, D. R. & Webb, W. W. Precise nanometer localization analysis for individual fluorescent probes. *Biophys. J.* **82,** 2775–83 (2002).

27. Barcellona, M. L., Cardiel, G. & Gratton, E. Time-resolved fluorescence of DAPI in solution and bound to polydeoxynucleotides. *Biochem. Biophys. Res. Commun.* **170,** 270–280 (1990).

28. Olivier, N., Keller, D., Rajan, V. S., Gönczy, P. & Manley, S. Simple buffers for 3D STORM microscopy. *Biomed. Opt. Express* **4,** 885 (2013).

29. Wade, R. H. On and around microtubules: an overview. *Mol. Biotechnol.* **43,** 177–91 (2009).

30. Pauleau, A.-L. & Erhardt, S. Centromere regulation: New players, new rules, new questions. *Eur. J. Cell Biol.* **90,** 805–810 (2011).

31. Maiato, H. *et al.* The ultrastructure of the kinetochore and kinetochore fiber in Drosophila somatic cells. *Chromosoma* **115,** 469–80 (2006).

32. Oliveira, R. A., Coelho, P. A. & Sunkel, C. E. The condensin I subunit Barren/CAP-H is essential for the structural integrity of centromeric heterochromatin during mitosis. *Mol. Cell. Biol.* **25,** 8971–84 (2005).

33. Milutinovich, M. & Koshland, D. E. Molecular biology. SMC complexes--wrapped up in controversy. *Science* **300,** 1101–2 (2003).

34. Ban, N. *et al.* Crystal structure of an idiotype-anti-idiotype Fab complex. *Proc. Natl. Acad. Sci. U. S. A.* **91,** 1604–8 (1994).

35. Yang, F., Moss, L. G. & Phillips, G. N. The molecular structure of green fluorescent protein. *Nat. Biotechnol.* **14,** 1246–51 (1996).

36. Oliveira, R. A. *et al.* Centromere-independent accumulation of cohesin at ectopic heterochromatin sites induces chromosome stretching during anaphase. *PLoS Biol.* **(submitted,** (2013).

37. Staudt, T., Lang, M. C., Medda, R., Engelhardt, J. & Hell, S. W. 2,2'-thiodiethanol: a new water soluble mounting medium for high resolution optical microscopy. *Microsc. Res. Tech.* **70,** 1–9 (2007).

38. Matsuda, A. *et al.* Condensed mitotic chromosome structure at nanometer resolution using PALM and EGFP- histones. *PLoS One* **5,** e12768 (2010).

39. Zessin, P. J. M., Finan, K. & Heilemann, M. Super-resolution fluorescence imaging of chromosomal DNA. *J. Struct. Biol.* **177,** 344–8 (2012).

40. Weiland, Y., Lemmer, P. & Cremer, C. Combining FISH with localisation microscopy: Super-resolution imaging of nuclear genome nanostructures. *Chromosome Res.* **19,** 5–23 (2011).

41. Flors, C. DNA and chromatin imaging with super-resolution fluorescence microscopy based on single-molecule localization. *Biopolymers* **95,** 290–7 (2011).

42. Aragon, L., Martinez-Perez, E. & Merkenschlager, M. Condensin, cohesin and the control of chromatin states. *Curr. Opin. Genet. Dev.* 1–8 (2013). doi:10.1016/j.gde.2012.11.004

43. Heidmann, D. *et al.* The Drosophila meiotic kleisin C(2)M functions before the meiotic divisions. *Chromosoma* **113,** 177–87 (2004).

44. Heeger, S. *et al.* Genetic interactions of separase regulatory subunits reveal the diverged Drosophila Cenp-C homolog. *Genes Dev.* **19,** 2041–53 (2005).

45. Bhatt, A. M. *et al.* The DIF1 gene of Arabidopsis is required for meiotic chromosome segregation and belongs to the REC8/RAD21 cohesin gene family. *Plant J.* **19,** 463–72 (1999).

46. Steffensen, S. *et al.* A role for Drosophila SMC4 in the resolution of sister chromatids in mitosis. *Curr. Biol.* **11,** 295–307 (2001).

47. Edelstein, A., Amodaj, N., Hoover, K., Vale, R. & Stuurman, N. Computer control of microscopes using μManager. *Curr. Protoc. Mol. Biol.* **Chapter 14,** Unit14.20 (2010).

48. Schindelin, J. *et al.* Fiji: an open-source platform for biological-image analysis. *Nat. Methods* **9,** 676–82 (2012).

49. Sooeet.com. Fast Fourier calculator. at <http://www.sooeet.com/math/fast-fourier-calculator.php>

Supplementary data

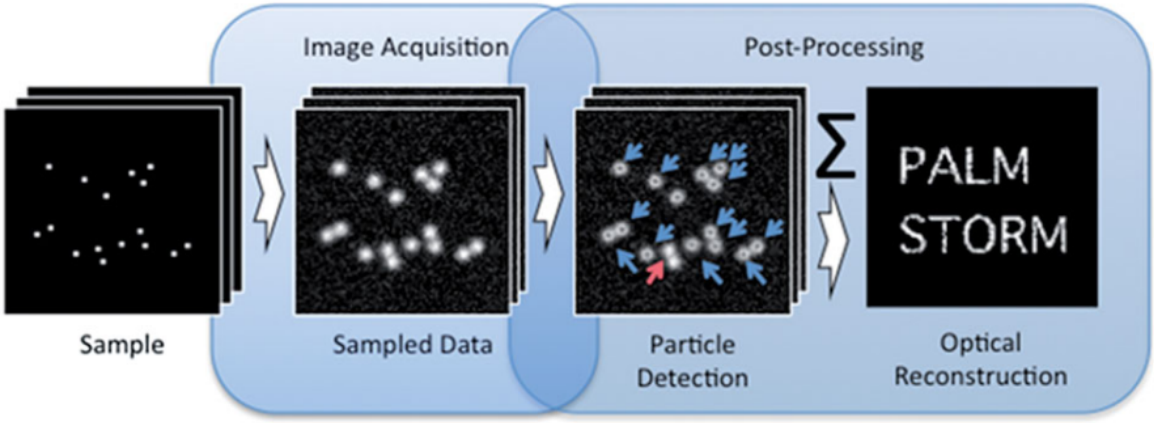

Sup. Fig. 1 - SML techniques are based making the population of fluorophores present in the sample go into a dark state and then making only a few emit. From a stack of images acquired while the sample was "blinking", single molecules are detected and their localizations used to reconstruct the sample with higher resolution than the input image stack. Adapted from[2].

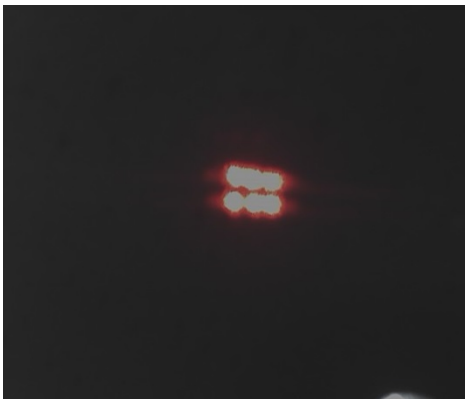

Sup. Fig. 2 – The KVANT laser has 6 beams and the 1 W specification applies only to the sum of all 6 beams, which means only 166 mW is available from each beam. However, only a single beam wsa utilized for the STORM system.

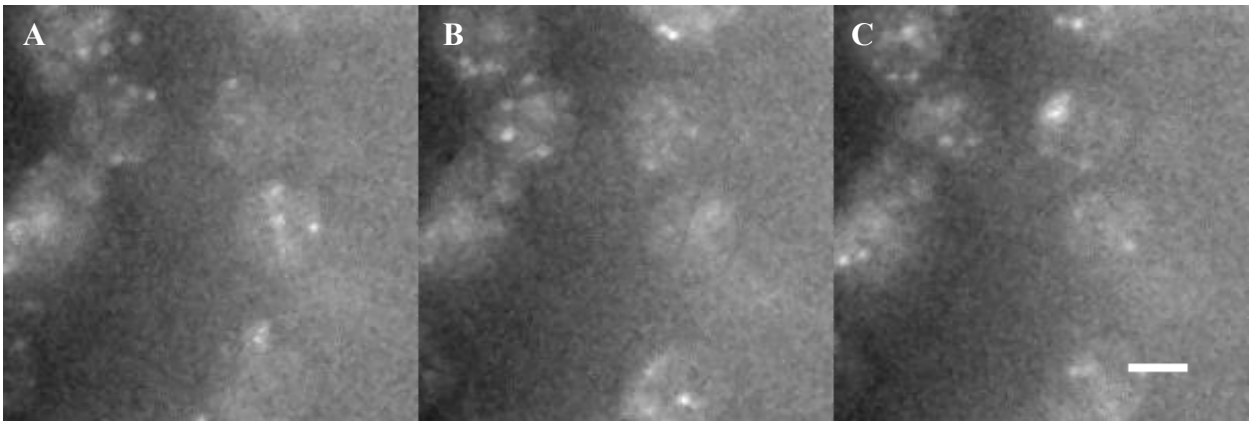

Sup. Fig. 3 – Blinking observed with the SPIM system. Frames A, B and C are from the beginning, middle and end of the stack, respectively. Blinks can be observed, but a high-background is present, making them harder to distinguish and lowering the resolution obtainable by super-resolution reconstruction. Scale bar – 2 μm.

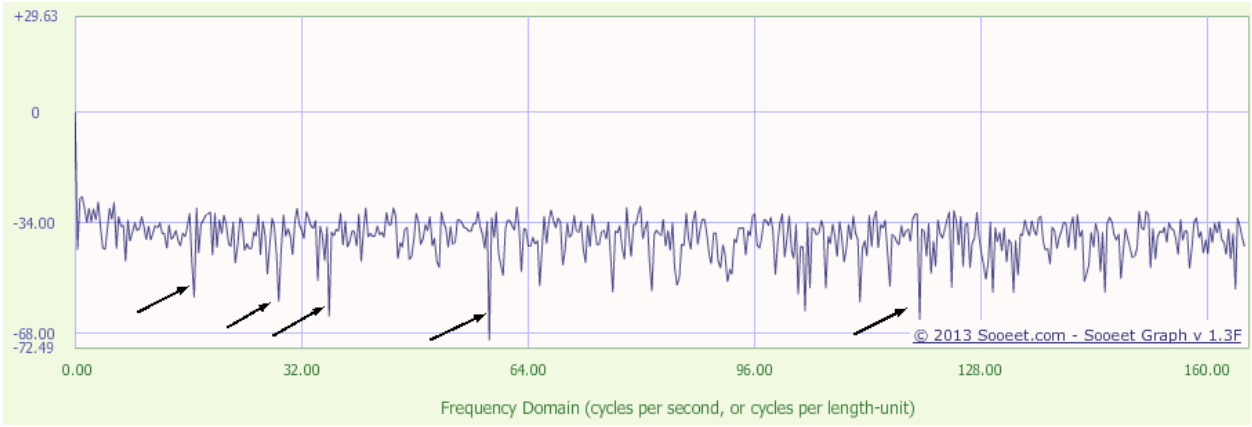

Sup. Fig. 4 – Sub-resolution frequencies present in the Nikon system, calculated as mentioned in Materials and Methods. Arrows correspond to vibrations present in the system. From left to right: 17Hz; 28Hz; 60Hz; 120Hz.

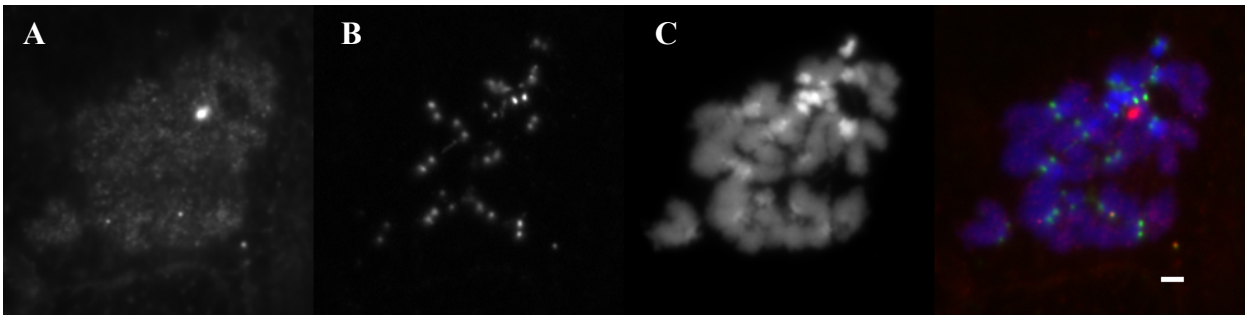

Sup. Fig. 5 – Failed SMC4 staining of S2 cells prepared by Cytospin. A- SMC4 with Alexa647; B – CENPC with FITC; C – DAPI; D - Merge of all three channels. Scale bar is 2 µm

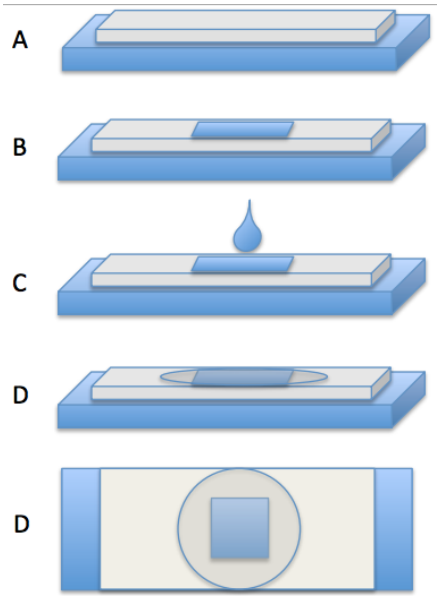

Sup. Fig. 6 – Mounting coverslips for imaging with the ROX buffer. A – A strip of parafilm is placed on top of a slide and heated so as to adhere to the glass; B – Once cold, a square of roughly 1cm^2 is cut from the slide; C – A drop of 20 µl of buffer is placed on the small square; D – The coverslip is placed on top of the square, as to cover it completely and sealed with nail-polish.